Experimental validation of a model of fan trailing-edge noise

Alain Guedel[a)], Yannick Rozenberg[b)], Michel Roger[c)] and Gérald Perrin[d)]

(Received: 14 March 2008; Revised: 18 November 2008; Accepted: 18 November 2008)

Broadband noise is a major part of the noise radiated by industrial and domestic fans. For low-speed fans broadband noise contribution to the overall A-weighted noise level is often much higher than that of the tonal noise at the blade passage frequency and its harmonics. One of the main mechanisms of broadband noise is trailing-edge noise, which is due to the convection of the turbulent flow past the blade trailing edge. This paper presents results of a research program in progress, which aims at validating a model that predicts broadband noise levels of rotating blades. Trailing-edge noise prediction is made using an analytical model deduced from an extension of Amiet's formulation. The input data to the model are the frequency spectrum and the spanwise correlation length scale of the wall pressure fluctuations on the blade suction side close to the trailing edge. This model was successfully validated on single fixed airfoils at different angles of attack in an anechoic wind tunnel. The input data were measured with wall pressure transducers on the airfoil suction side. In the present study, the validity of the trailing-edge noise model is assessed for a 800-mm axial flow fan which is used without casing in order to avoid the tip clearance noise contribution. Wall pressure fluctuations are measured with small pressure transducers flush mounted on two rotating blades, using a slip ring to transmit the pressure signals to the frequency analyser. A comparison of measured and predicted far-field sound pressure spectra at different observation angles is presented for two blade pitch angles 20° and 30°. The prediction proves to be quite good at 30° but strongly underestimates fan noise levels over a large frequency range at the lower blade angle. In this case another sound source related to the blade tip vortex is detected.

Primary subject classification: 11.4; Secondary subject classification: 21.6.5

1 INTRODUCTION

Broadband noise is a major part of the noise radiated by industrial and domestic fans. For low-speed fans broadband noise contribution to the overall A-weighted sound power level is indeed often much higher than the contribution of tonal noise at harmonics of the blade passage frequency. Different mechanisms contribute to fan broadband noise generation:

- interaction of blades with inflow turbulence
- trailing-edge noise
- vortex shedding noise
- tip vortex noise.

The first mechanism produces a major broadband noise contribution when the inlet flow turbulence is significant (turbulence intensity higher than 2 to 2.5%), which is the case for instance on an axial-flow fan behind a heat exchanger. Conversely, it becomes negligible compared with the other sources when the fan operates in a non-disturbed inlet flow field.

Vortex shedding noise, associated with von Karman vortices in the blade wake, occurs when the thickness of the blade trailing edge is larger than the boundary layer thickness. A sharp trailing edge is therefore beneficial to suppress this mechanism. Tip vortex noise, due to the complex flow pattern at the blade tip, associated with the pressure difference between the pressure and suction sides on axial fans, depends on the

[a)] CETIAT, 25, avenue des Arts, BP 52042, 69603 Villeurbanne cedex, FRANCE; email: alain.guedel@cetiat.fr.
[b)] ONERA, 29 avenue de la Division Leclerc, BP 72, 92322 Châtillon cedex FRANCE; email: yannick.rozenberg@onera.fr.
[c)] Ecole Centrale de Lyon, LMFA, 36, avenue Guy de Collongue, 69134 Ecully cedex, FRANCE; email: michel.roger@eclyon.fr.
[d)] CETIAT, 25, avenue des Arts, BP 52042, 69603 Villeurbanne cedex, FRANCE; email: gerald.perrin@cetiat.fr.

tip clearance and on the operating point. Typically, the noise level due to this mechanism decreases when the gap between the impeller and the casing is reduced.

Trailing-edge noise occurs when the turbulent boundary layer on the blade suction side is convected past the trailing edge, the turbulent energy of the wall pressure fluctuations being converted into acoustic energy that radiates to the far-field. This mechanism, which predominates over the other sources when the inlet turbulence intensity is low, corresponds to the minimum noise level radiated by a fan. For this reason, this paper is focussed on this last mechanism. The objective of the paper is to validate an analytical model of trailing-edge noise by comparison with experiment on rotating blades. The analytical model is briefly described in the first section. In the second section, the model is validated for a fixed inclined flat plate in an anechoic wind tunnel. In the third section, the validation is extended to a two-blade axial flow fan without shroud. Some working tracks to predict wall-pressure spectra on the blades are proposed in the fourth section. This could allow the creation of a full prediction of fan trailing-edge noise in the future. Summary of the main results and suggestions for future work are presented in conclusions.

2 TRAILING-EDGE NOISE MODEL

2.1 Stationary Airfoil

Trailing-edge noise predictions are made with an extension of Amiet's analytical formulation[1] for an isolated airfoil. The extension proposed by Roger and Moreau[2] accounts for the effects of a finite chord length and far-field radiation away from the mid-span plane. This model is detailed in Ref. 2 and in a previous NCEJ paper[3].

Only the main aspects are repeated here for conciseness and the related formulae are listed in the Appendix. According to Ref. 3, the far-field sound pressure spectrum radiated in the mid-span plane by a fixed airfoil in a uniform flow field can be expressed as:

$$S_{acou}(\vec{x},\omega) = \left(\frac{kc\,\sin\theta}{2\pi R}\right)^2 \times \frac{L}{2}\left|L'\left(x_1,\frac{\omega}{U_0},0\right)\right|^2 S_{wall}(\omega) l_y(\omega) \quad (1)$$

with:

S_{acou}: sound pressure spectrum (dB/Hz)
R: distance between the mid-span trailing edge and the observer (m)
x_1: coordinate of the observer along the airfoil chord
θ: angle between the chordwise and the observer directions (θ=0° *in the downstream direction*)
c: airfoil chord length (m)
L: airfoil span (m)
$|L'|$: aeroacoustic transfer function (see expression of L' in Appendix)
S_{wall}: spectrum of the wall-pressure fluctuations (dB/Hz)
l_y: spanwise correlation length scale of the wall-pressure fluctuations (m)
ω: angular frequency (rad/s)
k: acoustic wavenumber (m^{-1})
U_0: velocity of the uniform flow (m/s).

Equation (1) applies to a non-compact airfoil with large aspect ratio ($L/c > 1$). The equation is slightly more complicated for an airfoil of small aspect ratio and when the observer is away from the airfoil mid-plane[2].

The statistics of the turbulent wall-pressure fluctuations, namely the frequency spectrum and the spanwise correlation length scale, are the input data to the model. These quantities have to be assessed slightly upstream of the trailing edge for reasons detailed in Ref. 4.

The aeroacoustic transfer function L' between the turbulent wall-pressure fluctuations and the far-field sound pressure fluctuations is determined analytically on the basis of purely acoustic arguments. Its expression, given in the Appendix, is a function of chord length c, mean flow velocity U_0, convection velocity of the wall-pressure field near the trailing edge U_c, and frequency f. It has been shown equivalent to the use of a finite-chord Green's function as proposed by Howe[5] in the limit of vanishing Mach numbers.

2.2 Rotating Blade

At the low Mach numbers of interest, the aforementioned model may be extended to a rotating blade with the following adjustment, which is a simplified form of the transformation formulae already proposed by Paterson and Amiet[6]. The blade is split into several segments along its span and the airfoil theory is applied to each segment, assuming that the circular motion is locally equivalent to a translational motion. This assumption is reliable if the trailing-edge noise frequencies are much higher than the rotational frequency. The far-field sound radiation from a given rotating segment is obtained by averaging the sound pressure spectra radiated by the blade segment at several azimuthal locations, applying a Doppler factor to account for the relative motion of the source with respect to the observer. The flow velocity is assumed parallel to the chord line according to the weakly loaded airfoil assumption in the linearized theory.

As stated in Ref. 7, the transposition formula is written as:

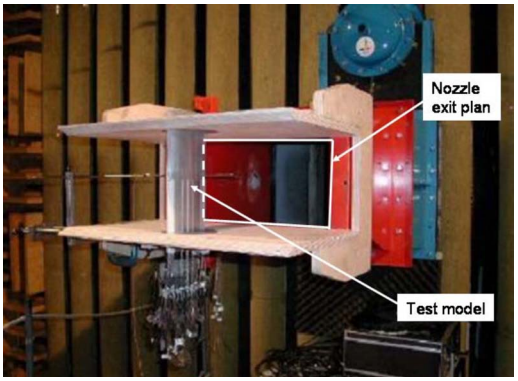

Fig. 1—Airfoil in the ECL anechoic wind tunnel.

$$S_{pp}(\vec{x},\omega)=\frac{B}{2\pi}\int_0^{2\pi}\frac{\omega_e(\Psi)}{\omega}S_{pp}^{\Psi}(\vec{x},\omega_e)d\Psi$$

$S_{pp}^{\Psi}(\vec{x},\omega_e)$ denotes the sound pressure spectrum that is radiated from the current blade segment at angle Ψ ignoring the Doppler frequency shift, and $\omega_e(\Psi)/\omega = 1+M\sin\Theta\sin\Psi = 1-M_r$, where (Θ,Ψ) are the radiation angle to the axis and the circumferential angle, respectively.

3 STATIONARY-AIRFOIL RESULTS IN WIND TUNNEL

3.1 Test Set-Up

In order to validate the trailing-edge noise model, experiments have been performed on airfoils of different shapes at various angles of attack in the large open-jet anechoic wind tunnel of Ecole Centrale de Lyon (ECL). Figure 1 shows a view of an airfoil in the wind tunnel.

The jet nozzle of the wind tunnel is rectangular with a height of 250 mm, corresponding to the airfoil span, and a width of 500 mm. The maximum flow velocity can exceed 40 m/s and the turbulence intensity in the potential core is lower than 0.8%. The background noise level of the facility is quite low (more than 10 dB below the noise radiated by the airfoil in the frequency range of interest).

The main broadband noise sources of the airfoil, vertically mounted in the wind tunnel, are trailing-edge noise and vortex shedding noise, since the two other broadband noise sources listed above have been suppressed. Interaction of the airfoil with inflow turbulence is negligible because of the low turbulence level of the jet flow, while tip vortex noise is eliminated by the horizontal side-plates fixed on the nozzle lips (see Fig. 1).

The airfoil is instrumented with flush-mounted fluctuating pressure transducers to measure the wall-pressure spectra and correlation length scales near the trailing edge.

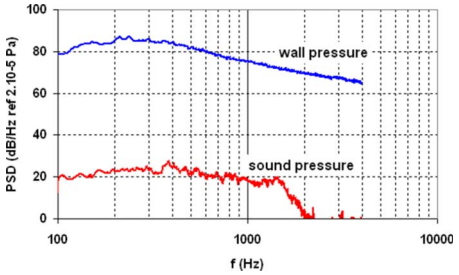

Fig. 2—Wall pressure and sound pressure spectra measured on a flat plate with 5° incidence, V=20 m/s. Far-field microphone at R=2 m, θ=90°.

A far-field microphone is moved in the airfoil mid-span plane at discrete positions on a circle of 2-meter radius centered at the trailing-edge mid-span.

3.2 Validation of the Model

The analytical model has been validated on different airfoils such as a NACA 0012 (100 mm chord length), two airfoils designed by VALEO and a flat plate (100 mm chord length and 3 mm constant thickness). The following figures show results obtained on the flat plate at different angles of attack. All the spectra presented here are narrowband and refer to Power Spectral Density (PSD). An example of wall pressure spectrum measured on the plate suction side close to the trailing edge is given in Fig. 2 for a 5° angle of attack and a flow velocity of 20 m/s. This spectrum is compared to the PSD of the far-field sound pressure signal measured at a distance R=2 meters from the plate in the mid-span plane and at an observation angle θ=90° (direction normal to the plate). Coherence functions γ^2 of the wall pressure signals in the

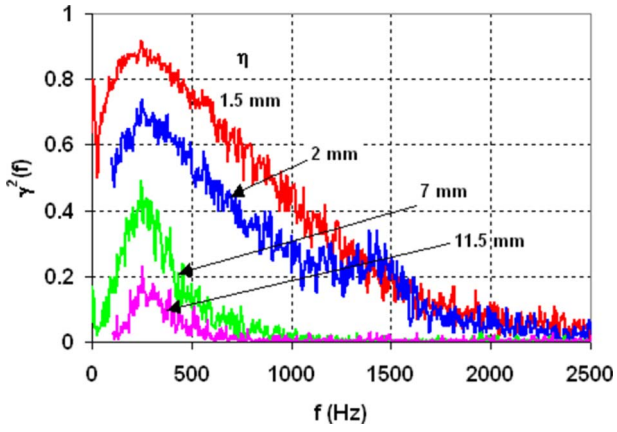

Fig. 3—Coherence function of the wall pressure fluctuations as a function of the spanwise distance η between the pressure transducers. Flat plate with 5° incidence, V=20 m/s.

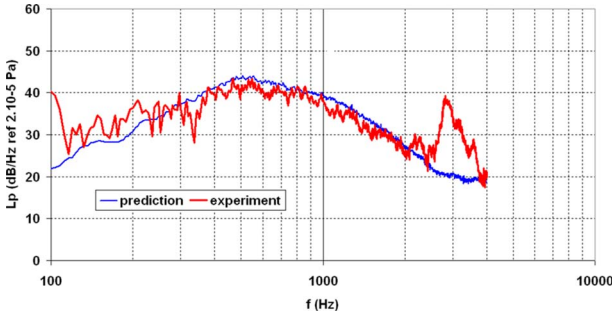

Fig. 4—Comparison of measured and predicted narrowband sound pressure spectra. Flat plate with 5° incidence, V=40 m/s, θ =90°.

spanwise direction are shown in Fig. 3 for the flat plate at 5° angle of attack as a function of the distance η between the pressure transducers. From this information we can calculate the spanwise correlation length scales $l_y(\omega)$ of the model (see Sec. 4.2).

Comparisons of the predicted and measured far-field sound pressure spectra for the flat plate positioned at two angles of attack (5° and 10° respectively) and at an observation angle θ=90° are shown in Figs. 4 and 5. The prediction is close to the experiment, except around 2.7 kHz at 5° incidence, where the hump observed on the measured spectrum is due to vortex shedding noise, which is not considered in the present model. This hump completely disappears at 10° incidence because the boundary layer on the suction side of the flat plate becomes much thicker than the trailing edge.

The trailing-edge noise model may be considered as fully validated on a fixed airfoil provided the input data to the model are accurately assessed. It is worth noting that sound scattering at the nozzle lips, not included in the model, may be responsible for some local discrepancies in the spectral comparison. The same overall

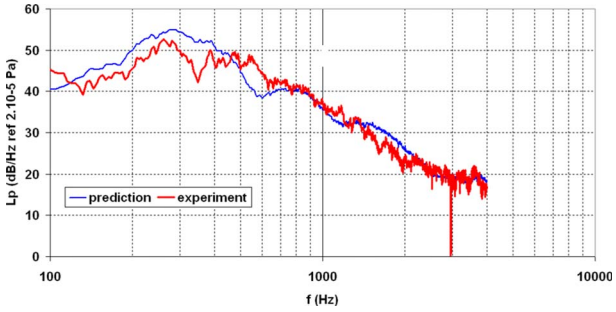

Fig. 5—Comparison of measured and predicted narrowband sound pressure spectra. Flat plate with 10° incidence, V=40 m/s, θ =90°.

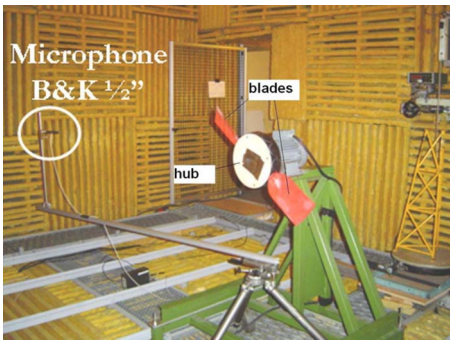

Fig. 6—Test fan in anechoic chamber.

agreement has been obtained on the flat plate for other observation angles and angles of attack as well as on other airfoil shapes.

4 RESULTS ON ROTATING BLADES

4.1 Experimental Set-Up

The selected fan is an axial-flow fan of 800-mm diameter (Fig. 6). It has only two blades to avoid the potential noise source arising from blade interactions. Furthermore, the fan casing has been removed to avoid the noise related to the disturbed flow in the radial tip clearance.

The blades made of plastic have the following geometrical characteristics:

- tip radius: 400 mm
- hub radius: 135 mm
- tip chord length: 135 mm (chord length nearly constant along the span)
- maximum thickness: 4 mm
- blade pitch angle: adjustable from 15 to 35° (values at the blade tip).

A variable-speed motor is used to drive the fan. The reference speed for all the tests was 600 rpm. Each of the two blades is equipped with 6 flush-mounted microphones in order to measure the spectra and spanwise correlation length scales of the wall-pressure fluctuations at two radial locations (at mid-span and near the blade tip) on the blade suction side, close to the trailing edge (Fig. 7). The microphones embedded within the

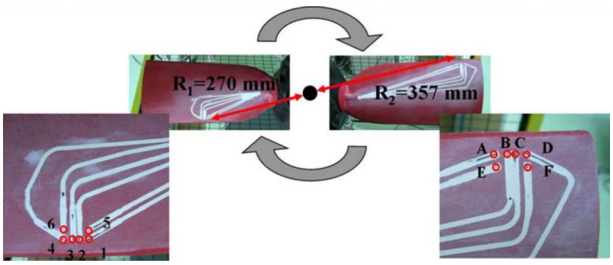

Fig. 7—Flush-mounted microphones on the blades.

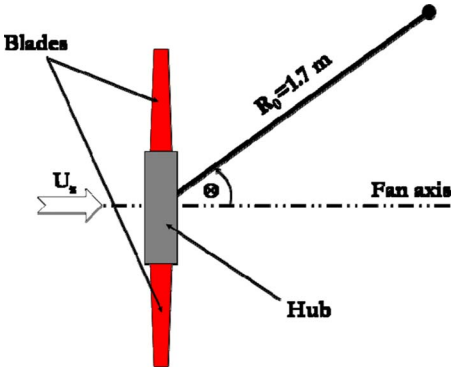

Fig. 8—Directivity set-up.

blades have a diameter and a length of 2.5 mm. The signals from the rotating sensors are transmitted to the analyser via a 14-channel slip ring. The effect of this device on the signals is assumed to be insignificant. The detailed layout of the sensors on the blades and the calibration procedure are described in Ref. 7. The far-field noise directivity of the fan is measured with a half-inch microphone moved on a rotating boom in a horizontal plane at 1.7 m from the impeller center (Fig. 8).

4.2 Validation of the Model

The validity of the trailing edge noise prediction model was tested for two blade pitch angles β_0=20 and 30°. It was observed that the measured far-field spectra at these two blade settings were quite different in the mid-frequency range between 1 and 3 kHz (Fig. 9), the level being much higher for β_0=20°. This hump was also observed for β_0=15° and 25°, but with amplitude lower than for the 20° blade setting.

As observed in Fig. 10, the wall-pressure spectra measured at mid-span with the blade sensors do not show such a difference between the two blade angles. It is shown in the next section that an additional noise source may be responsible for the hump in the mid-frequency range of the spectrum, for the 20° blade setting.

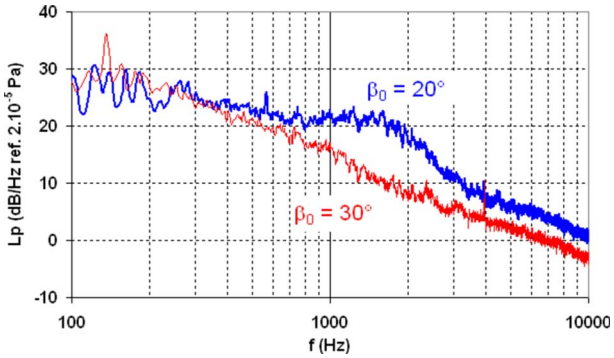

Fig. 9—Measured narrowband sound pressure spectra, β_0=20 and 30°, Θ=90°.

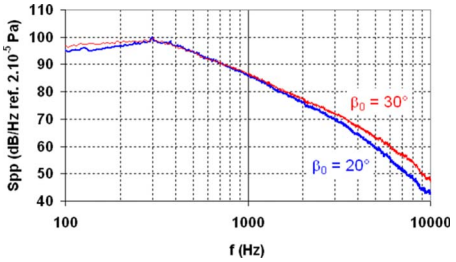

Fig. 10—Wall-pressure fluctuation narrowband spectra at mid-span, β_0=20 and 30°.

The spanwise correlation length, which is characteristic of the spanwise size of the turbulent eddies convected in the blade boundary layer, is defined by:

$$l_y(\omega) = \int_0^\infty \sqrt{\gamma^2(\omega,\eta)}\,d\eta \qquad (2)$$

with:

- l_y: spanwise correlation length (m)
- ω: angular frequency (rad/s)
- γ^2: coherence function
- η: spanwise separation between wall microphones (m)

Figure 11 shows the coherence functions of the wall-pressure fluctuations measured on the blade close to the tip for β_0=30°. Above about 300 Hz the coherence decreases with both frequency and separation η between the wall microphones. In this frequency range Corcos' model[8] applies. With this model the coherence function may be written as:

$$\gamma^2(\omega,\eta) = e^{-2\omega/b_c U_c \eta} \qquad (3)$$

where:

- b_c: empirical coefficient adjusted to the measurements.
- U_c: convection velocity of the wall-pressure fluctuations (m/s).

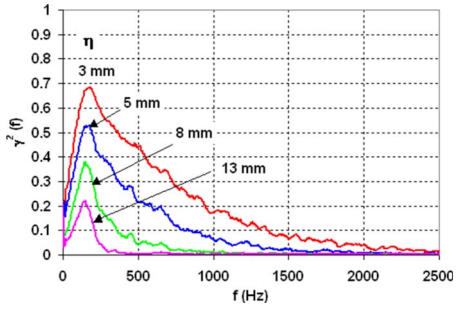

Fig. 11—Spanwise coherence functions of the wall pressure fluctuations near the blade tip. β_0=30°.

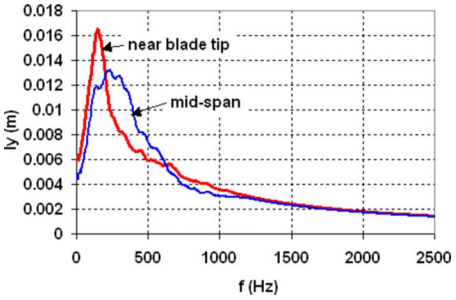

Fig. 12—Spanwise coherence length scales of the wall pressure fluctuations at mid-span and near the blade tip. $\beta_0=30°$.

From Eqns. (2) and (3), the correlation length can be expressed as:

$$l_y(\omega) = \frac{b_c U_c}{\omega} \qquad (4)$$

The values of b_c and U_c are deduced from the wall-pressure measurements, and it was determined that $b_c \approx 1.4$ and $U_c \approx 0.75 \times 2\pi RN$ for both radial locations R of the two sets of pressure sensors.

The frequency of the maximum of γ^2 in Fig. 11 corresponds to the frequency of the biggest turbulent eddies in the blade boundary layer[7]. Below this frequency Corcos' model does not apply any more and l_y is deduced from Eqn. (2) with a numerical integration of the experimental data. The use of Corcos' model in the frequency range above the peak of coherence avoids uncertainties in l_y assessment due to uncertainties in the coherence function measured at high frequency.

Spanwise coherence length scales of the wall-pressure fluctuations at mid-span and near the tip are shown in Fig. 12 for $\beta_0=30°$. These data are similar to those that would be measured on a fixed 2D airfoil in a uniform flow at the corresponding radial blade velocity.

Figure 13 shows a comparison of the measured and predicted far-field sound pressure spectra for $\beta_0=30°$ and two microphone angles $\Theta=40$ and 90°. Note that to obtain the predicted data, the blade was divided into nine spanwise segments, the width of which is larger than the spanwise correlation length scale. The prediction for $\beta_0=30°$ may be considered as quite satisfactory, considering that the wall-pressure statistics used in the model is only known at two spanwise locations (for mechanical reasons, it was not possible to insert more than six pressure sensors on each blade). An extrapolation procedure was used to obtain the input data for each of the nine blade segments[7].

The prediction obtained for $\beta_0=20°$ (not shown) is poor since it does not capture the hump observed on the

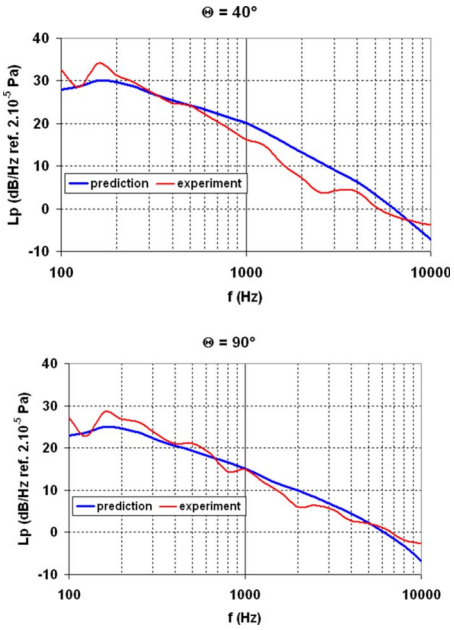

Fig. 13—Comparison of predicted and measured narrowband sound pressure spectra, $\beta_0=30°$, $\Theta=40$ and 90°.

measured spectra in the mid-frequency range. The next step, detailed below, is to find the origin of this hump.

4.3 Origin of the Hump in the Noise Spectrum for $\beta_0=20°$

A vortex-shedding noise mechanism was first suspected to explain the origin of the hump. The increase of the noise level in this specific frequency range was indeed in agreement with a Strouhal number $St=fh/U=0.2$, where h is the blade trailing edge thickness and U the tangential velocity. This velocity varies in the spanwise direction, which explains the broadband shape of the resulting spectrum compare to the narrowband peak observed for the fixed 2D airfoil case, at low angle of attack (Fig. 4).

A modification of the blade trailing edge was made with an adhesive tape used as a zero-thickness blade extension, but the radiated noise spectrum remained unchanged, which eliminated the vortex shedding as the possible cause for this hump.

A possible Tolmien-Schlichting instability phenomenon could also explain this spectrum. Triggering the boundary layer transition with trip wires fixed on the blade span at several chordwise locations on the pressure and suction sides successively invalidated this hypothesis.

Finally, some modifications of the blade-tip geometry had an influence on the medium frequency band of the spectrum for $\beta_0=20°$, suggesting that the tip vortex is responsible for this noise at this blade angle. Tuft flow visualisations with ostrich hurl

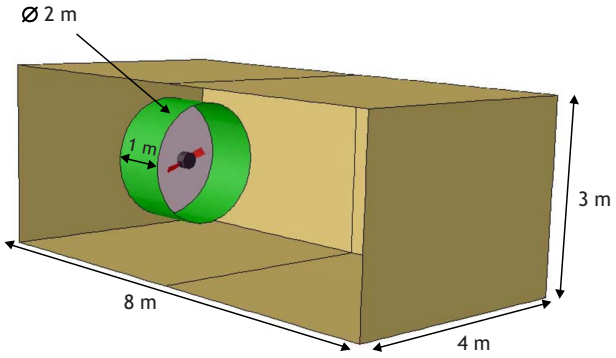

a)

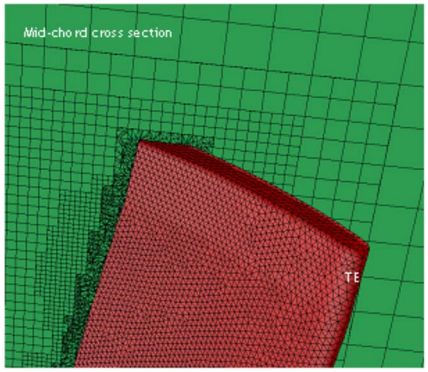

b)

Fig. 14—Mesh used in the URANS simulations.

arranged near the blade tip showed that the tip vortex is clearly different for β_0=20 and 30°. For 20° blade setting the vortex followed the blade tip over three quarters of the chord length, whereas for 30° the vortex was detached much closer to the leading edge.

CFD calculations with Fluent were also used to understand the difference in the tip vortex flow pattern between the two blade settings and confirmed this point. An Unsteady RANS ("URANS") simulation with a model for the turbulent kinetic energy and dissipation $(\tilde{k}, \tilde{\varepsilon})$ was carried out on the impeller installed in a closed box, simulating the experimental room. Figures 14(a) and 14(b) show (a) the calculation domain with the outer surface of the sliding mesh and the surrounding walls, and (b) a view of the unstructured grid (on a portion of the blade surface and mid-chord section). The overall mesh includes 2.6 million cells.

Figure 15 shows for both blade angles, the computed static pressure contours and flow path lines at the blade tips on the suction side. Flow separation is identified via the zone of minimum static pressure. For β_0=30°, the blade tip vortex is detached near the mid-chord, whereas this separation occurs closer to the trailing edge for β_0=20°. Other results of practical interest could be deduced from the URANS simulations, but they are beyond the scope of the present paper.

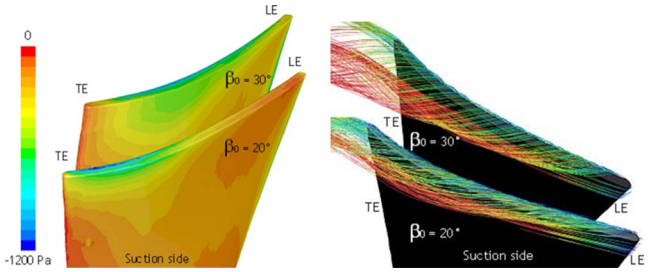

Fig. 15—Computed static pressure contours and flow path lines on the blade suction side close to the blade tip, β_0=20 and 30°.

5 PROGRESS ON WALL-PRESSURE SPECTRUM PREDICTION

The wall-pressure spectrum just upstream of the trailing edge is the main input data of the model proposed by Amiet. As it is influenced by the velocity fluctuations in all parts of the boundary layer, it can be considered as a non-local variable, tricky to determine. The present study resorts to an experimental approach chosen for the sake of validation. Further applications for design purposes would require a complete prediction strategy including the determination of both the sources and the acoustic field. Highly intensive computations such as Large Eddy Simulations provide the needed wall-pressure statistics but are too time consuming to be used in an industrial context. RANS (Reynolds-Averaged Navier-Stokes) simulations are more currently used but they do not directly give information on the wall-pressure fluctuations. Some additional relevant scaling laws have therefore to be introduced to infer this information from the computations.

5.1 Zero-Pressure Gradient Case

A two-layer model is often used to characterize the large ranges of relevant length, velocity and pressure scales in a turbulent boundary layer. The inner layer called the viscous sub-layer addresses the flow near the wall and the outer layer the remaining part. Based on this description, Keith et al.[9] compared the wall-pressure spectra from various experiments in a normalized form.

The high-frequency range collapses when normalized by inner-layer scales, such as the wall shear stress τ_w and the ratio ν/u_τ^2. For low frequencies, a collapse is ensured by outer-layer scaling with the external velocity U_e and the boundary-layer thickness δ or the boundary-layer displacement thickness δ^*.

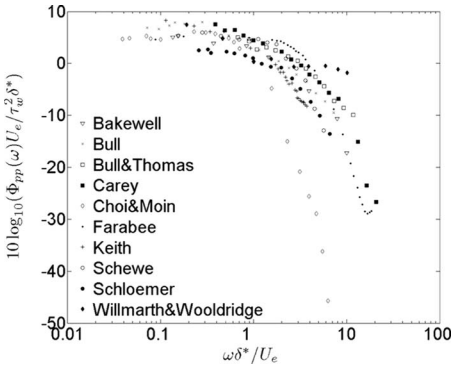

Fig. 16—Normalized wall pressure spectra using mixed variables.

This mixed normalization is efficient for different experimental results, as shown in Fig. 16. The spectra presented in this figure have been measured beneath flat-plate or channel boundary layers for which the mean pressure is considered as constant. The discrepancies observed at high frequencies are attributed by Goody[10] to a Reynolds-number effect. Based on a similar scaling law, Goody developed a semi-empirical spectral model, taking into account the influence of the Reynold number at high frequencies, as shown in Fig. 17. Knowing the mixed parameters, thanks to a RANS simulation and an appropriate post-processing, the wall-pressure spectra for a zero-pressure gradient flow can be determined.

5.2 Pressure Gradient Case

The boundary layers on the suction side of real blades encounter an adverse pressure gradient, modifying the wall-pressure statistics, as observed experimentally by Schloemer[11] and numerically by Na[12]. In the presence of a strong adverse pressure gradient, the relative increase of wall-pressure amplitude can reach 10 dB and has to be taken into account. Based on a semi-empirical approach, Rozenberg[13] proposed a first attempt to improve Goody's model, including the pressure gradient effects. Further studies are still needed to confirm the validity of the normalization over a wider range of pressure-gradient parameters. As a consequence, for fan-noise predictions in industrial context former models, such as that of Chase[14] which uses wall-pressure spectra for flat-plate boundary layers, may seriously underestimate the actual noise level. The chordwise pressure gradient on the blades must be accounted for explicitly.

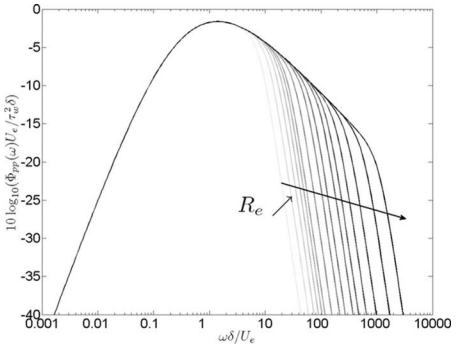

Fig. 17—Goody's wall pressure spectra expressed with mixed parameters for increasing Reynolds numbers.

6 CONCLUSIONS

An analytical model aimed at predicting the trailing-edge noise radiated by fan blades has been validated. A specific experimental set-up with embedded pressure sensors on two rotating blades was designed to collect the input data of the model. A good agreement was obtained between the measured and predicted far-field sound pressure spectra when the trailing-edge noise mechanism is predominant. A tip noise mechanism was detected at low blade pitch angles, which is not predicted by the present model.

Further work is needed to check the validity of the prediction on axial flow fans with casing. This will imply a measure or an estimation of the input data required by the model. This study also indicated that accounting for other self-noise mechanisms (such as tip vortex noise) may sometimes be necessary to improve the prediction.

7 APPENDIX

Expressions of the aeroacoustic transfer function have been given in Refs. 2 and 3 and are listed below for completeness.

$$L' = L'_1 + L'_2$$

$$L'_1 = -\frac{e^{2iC}}{iC}\left\{(1+i)e^{-2iC}\sqrt{\frac{B}{B-C}}E^*[2(B-C)] - (1+i)E^*[2B] + 1\right\}$$

$$\frac{1}{H}L'_2 = \{e^{4i\mu}[1-(1+i)E^*(4\mu)]\}^c - e^{2iD} + i[D + K_1^* + (M_0-1)\mu]G$$

$$G = (1+\varepsilon)e^{i(2\mu+D)}\frac{\sin(D-2\mu)}{D-2\mu} + (1-\varepsilon)$$
$$\times e^{i(-2\mu+D)}\frac{\sin(D+2\mu)}{D+2\mu}\cdots$$
$$+\frac{(1+\varepsilon)(1-i)}{2(D-2\mu)}e^{4i\mu}E^*[4\mu]$$
$$-\frac{(1-\varepsilon)(1+i)}{2(D+2\mu)}e^{-4i\mu}E[4\mu]\ldots+\frac{e^{2iD}}{2}\sqrt{\frac{2\mu}{D}}E^*[2D]$$
$$\times\left[\frac{(1+i)(1-\varepsilon)}{D+2\mu}-\frac{(1-i)(1+\varepsilon)}{D-2\mu}\right]$$

$$H=\frac{(1+i)e^{-4i\mu}(1-\Theta^2)}{2\sqrt{\pi}(\alpha-1)K_1^*\sqrt{B}} \quad K_1=\frac{\omega c}{2U_c}$$
$$\varepsilon=\left(\sqrt{1+\frac{1}{4\mu}}\right)^{-1}$$

$$B=K_1+(M_0+1)\mu \quad C=K_1-\left(\frac{x_1}{S_0}-M_0\right)\mu$$
$$D=\mu\left(1-\frac{x_1}{S_0}\right)$$

$$S_0^2=x_1^2+\beta_0^2(x_2^2+x_3^2) \quad \mu=\frac{K_1M_0}{\beta_0^2}$$
$$\Theta=\sqrt{\frac{\alpha K_1+(1+M_0)\mu}{K_1+(1+M_0)\mu}}$$

$$E^*[x]=\int_0^x\frac{e^{-it}}{\sqrt{2\pi t}}dt$$

Here U_c is the convection speed of the boundary layer disturbances, with $\alpha=U_0/U_c$. The second term can be ignored for simplicity, except at lower frequencies.

8 REFERENCES

1. R. K. Amiet "Noise due to turbulent flow past a trailing edge", *J. Sound Vib.*, **47**(3), 387–393, (1976).
2. M. Roger and S. Moreau "Back-scattering correction and further extensions of Amiet's trailing-edge noise model. Part 1: theory", *J. Sound Vib.*, **286**(3), 477–506, (2005).
3. M. Roger, S. Moreau and A. Guedel "Broadband fan noise prediction using single-airfoil theory", *Noise Control Eng. J.*, **54**(1), 5–14, (2006).
4. T. F. Brooks and T. H. Hodgson "Trailing-edge noise prediction from measured surface pressures", *J. Sound Vib.*, **78**(1), 69–117, (1981).
5. M. S. Howe "Edge-source acoustic Green's function for an airfoil of arbitrary chord with application to trailing-edge noise", *Q. J. Mech. Appl. Math.*, **54**(1), 139–155, (2001).
6. R. W. Paterson and R. K. Amiet "Noise of a model helicopter rotor due to ingestion of turbulence", NASA CR-3213, (1979).
7. Y. Rozenberg, M. Roger, A. Guédel and S. Moreau "Rotating blade self noise: Experimental validation of analytical models", *AIAA Pap.* 2007–3709, (2007).
8. G. M. Corcos "The structure of turbulent pressure field in boundary-layer flows", *J. Fluid Mech.*, **18**, 53–378, (1964).
9. W. L. Keith, D. A. Hurdis and B. M. Abraham "A comparison of turbulent boundary layer wall-pressure spectra", *J. Fluids Eng.*, **114**(3), 338–347, (1992).
10. M. Goody "Empirical spectral model of surface pressure fluctuations", *AIAA J.*, **42**(9), 1788–1794, (2004).
11. H. H. Schloemer "Effects of pressure gradients on turbulent-boundary-layer wall-pressure fluctuations", *J. Acoust. Soc. Am.*, **42**(1), 93–113, (1967).
12. Y. Na "Direct numerical simulation of turbulent boundary layers with adverse pressure gradient and separation", PhD dissertation, Stanford University, (1996).
13. Y. Rozenberg "Modélisation analytique du bruit aérodynamique à large bande des machines tournantes: utilisation de calculs moyennés de mécanique des fluides", PhD dissertation, Ecole Centrale de Lyon, (2007).
14. D. M. Chase "Modeling the wavevector-frequency spectrum of turbulent boundary layer wall pressure", *J. Sound Vib.*, **70**(1), 29–67, (1980).